Heliyon 10 (2024) e29297

Contents lists available at ScienceDirect

Heliyon

journal homepage: www.cell.com/heliyon

Research article

# Evaluation of core-shell $Fe_3O_4$@Au nanoparticles as radioenhancer in A549 cell lung cancer model

Youssef Slama [a,b,*], Angelique Arcambal [a], Axelle Septembre-Malaterre [a], Anne-Laure Morel [c], Sabrina Pesnel [c], Philippe Gasque [a]

[a] Université de La Réunion, Unité de Recherche Etudes Pharmaco-Immunologiques (EPI), CHU de La Réunion, Site Felix Guyon, Allée des Topazes, SC11021, 97400, Saint-Denis, La Réunion, France
[b] Clinique Sainte-Clotilde, Groupe Clinifutur, 127 Route de Bois de Nèfles, 97400, Saint-Denis, La Réunion, France
[c] Torskal, Nanosciences, 2 Rue Maxime Rivière, 97490 Sainte-Clotilde, La Réunion, France

ARTICLE INFO

*Keywords:*
$Fe_3O_4$@Au nanoparticle
Radiotherapy
Lung cancer
Oxidative stress
Pro-inflammatory response
Cell death

ABSTRACT

In radiotherapy, metallic nanoparticles are of high interest in the fight against cancer for their radiosensitizing effects. This study aimed to evaluate the ability of core-shell $Fe_3O_4$@Au nanoparticles to potentiate the irradiation effects on redox-, pro-inflammatory markers, and cell death of A549 human pulmonary cancer cells. The hybrid $Fe_3O_4$@Au nanoparticles were synthesized using green chemistry principles by the sonochemistry method. Their characterization by transmission electron microscopy demonstrated an average size of 8 nm and a homogeneous distribution of gold. The decreased hydrodynamic size of these hybrid nanoparticles compared to magnetite ($Fe_3O_4$) nanoparticles showed that gold coating significantly reduced the aggregation of $Fe_3O_4$ particles. The internalization and accumulation of the $Fe_3O_4$@Au nanoparticles within the cells were demonstrated by Prussian Blue staining. The reactive oxygen species (ROS) levels measured by the fluorescent probe DCFH-DA were up-regulated, as well as mRNA expression of SOD, catalase, GPx antioxidant enzymes, redox-dependent transcription factor Nrf2, and ROS-producing enzymes (Nox2 and Nox4), quantified by RT-qPCR. Furthermore, irradiation coupled with $Fe_3O_4$@Au nanoparticles increased the expression of canonical pro-inflammatory cytokines and chemokines (TNF-α, IL-1β, IL-6, CXCL8, and CCL5) assessed by RT-qPCR and ELISA. Hybrid nanoparticles did not potentiate the increased DNA damage detected by immunofluorescence following the irradiation. Nevertheless, $Fe_3O_4$@Au caused cellular damage, leading to apoptosis through activation of caspase 3/7, secondary necrosis quantified by LDH release, and cell growth arrest evaluated by clonogenic-like assay. This study demonstrated the potential of $Fe_3O_4$@Au nanoparticles to potentiate the radiosensitivity of cancerous cells.

## 1. Background

Cancer, known as a major burden of disease worldwide, with nearly 10 million deaths in 2020, is one of the greatest public health challenges [1]. Importantly, the global market for cancer therapies reached US$196 billion in 2023 and is expected to reach US$375 billion by 2027 [2]. The increase in the market size of cancer therapies demonstrates the need and interest to develop new therapies

* Corresponding author. Clinique Sainte-Clotilde, Groupe Clinifutur, 127 Route de Bois de Nèfles, La Réunion, 97400, Saint-Denis, France.
*E-mail address:* youssef.slama@clinifutur.net (Y. Slama).

https://doi.org/10.1016/j.heliyon.2024.e29297
Received 14 June 2023; Received in revised form 3 April 2024; Accepted 4 April 2024
Available online 5 April 2024

and/or improve existing ones to control tumors. Furthermore, it has been reported that without significant efforts to improve global cancer control, mortality by cancer could reach up to 12.9 million/year by 2030 [3]. Many treatments have been developed to reduce cancer deaths and improve patient lives. Among these therapies, radiotherapy preconized for more than 50 % of patients, is a major and effective approach for killing or controlling tumors. Ionizing radiation used in radiotherapy can cause direct damage to DNA molecules, leading to cell cycle arrest and decreased proliferation. By indirect effects, ionizing radiation promotes cell necrosis and apoptosis by increasing reactive oxygen species (ROS) production through water radiolysis and endogenous oxidative stress [4–6]. Radiotherapy also promotes a pro-inflammatory response through the release of pro-inflammatory cytokines [7,8]. The oxidative stress associated with the pro-inflammatory response will engage apoptosis/necrosis pathways [5,6,9].

However, radiotherapy also involves limitations comprising radio-induced toxicities on healthy surrounding tissues and an increase in the risk of developing radio-induced cancer following an exposition to a high dose of radiation [10,11]. Moreover, radiotherapy remains limited for tumors difficult to target or those requiring high doses of radiation, such as radioresistant cancers, which often leads to decreased therapeutic outcomes and cancer reoccurrence [12,13].

Noticeably, the delivered dose by radiotherapy is directly related to the nature of the crossed tissue. In the case of non-small cell lung cancer (NSCLC), the current clinical treatment planning tools are limited by the heterogeneity of lungs for the delivered dose calculation due to the air in the alveoli and the low density of surrounding tissue [14,15]. However, studies have reported an enhancement of overall survival associated with increased delivered doses in NSCLC. The main challenge in radiotherapy concerns the balance between eradicating tumor cells and sparing normal tissue. In this context, improving the radiotherapy protocols represents a real challenge.

Interestingly, new therapeutic tools, namely radiosensitizers, potentiate the deleterious effects of radiation without elevating the delivered doses and the associated toxicities [16,17].

These radiosensitizers are considered to complete existing approaches allowing better targeting of tumor tissues and more localized and consolidated damage. They could exhibit attractive therapeutic advantages in acquired/intrinsic radioresistant cancers involving heterogeneous tissues, such as NSCLC, by reducing toxicity risks in normal tissues while maintaining the tumoricidal effect. As such, metallic nanoparticles coupled to irradiation present a high radiosensitizing potential depending on the cellular type studied [18]. The nanometric size (1–100 nm) of metallic nanoparticles increases the permeability and retention rate of the tumoral cells, allowing their accumulation in tumor cells [19]. The ionizing radiation will interact with high-atomic number (Z) atoms in the nanoparticles, generating secondary photoelectrons promoting additional ROS production [9,20]. Thus, metallic nanoparticles based on gold (Au), silver, or iron amplify the therapeutic potential of irradiation on redox homeostasis, mitochondria functions, cell cycle, and cell proliferation. Thus, nanoparticles promote autophagy, apoptosis, or tumor cell necrosis, prolonging tumor-bearing mice's median survival time [9,20,21].

AuNPs are attracting considerable interest as a therapeutic or medical imaging agent for magnetic resonance imaging, due to their unique physicochemical properties and biocompatibility [22,23]. Additionally, several novel and highly efficient contrast agents based on $Fe_3O_4$ nanoparticles were recently reported but $Fe_3O_4$ nanoparticles also present disadvantages related to their poor stability and high toxicity for cells [24,25].

Thus, synthesizing nanoparticles of $Fe_3O_4$ embedded into gold shells appears strategic due to $Fe_3O_4$ superparamagnetism and the gold's optical properties. Moreover, gold shell helps ensure the components' stability of $Fe_3O_4$ by reducing toxicity, excessive aggregation, as well as acid and oxidative degradation [3,26–28].

The use of nanotechnologies in medical research is highly promising. However, clinical translation is still complicated due to the lack of data concerning nanomaterials' interactions with biological entities and a lack of correlation between *in vitro* and *in vivo* studies. Furthermore, the large-scale production of nanomaterials for commercialization remains technically difficult, expansive and associated with high ecotoxicological risks [29,30].

In this context, the present study aims to evaluate the potential of $Fe_3O_4$@Au nanoparticles to amplify the effect of ionizing radiation (high energy 6 megavoltage photon beam) applied in clinical radiotherapy on pulmonary carcinoma A549 *in vitro*. Several redox, pro-inflammatory markers, and cell death were evaluated. This core-shell nanoparticle associates $Fe_3O_4$ atoms with gold atoms to combine their radio-sensitizing effects while limiting toxicity risks. The hybrid nanoparticles studied in the present work were synthesized using green chemistry principles, consistently with environmental concerns about nanomaterial large-scale production.

Main studies published on the radio-sensitizing effect of metallic nanoparticles combined with ionizing radiation involve low-energy external beam X-rays (kilovoltage). It seems crucial to evaluate the cellular impact of nanoparticles combined with radiotherapy using the energy of treatment currently applied during a clinical radiotherapy routine.

Moreover, this work will help to increase understanding of the biological effect of metallic nanoparticles coupled to ionizing radiation, such as the inflammatory response and redox modulation, particularly in the case of cancers implicating heterogeneous tissues such as NSCLC.

## 2. Methods

### 2.1. Synthesis of $Fe_3O_4$@Au nanoparticles

Concerning the process of nanoparticle synthesis, they were produced according to the patent FR2200483 established by « Morel Anne-Laure, Ben Haddada Maroua, Nikitenko Serguei, Chave Tony, 2022, synthèse assistée par ultrasons de nanoparticules constituées d'un cœur ferrique recouvert d'or». Firstly, the synthesis of $Fe_3O_4$ nanoparticles was performed according to the method previously described by Morel et al. [31] by substituting hydrazine and ammonia with a sonochemical approach to follow the principles of green

chemistry.

In the second step of the synthesis, a 0.05 M solution of L-cysteine (L-cys) was prepared by dissolving L-cystein hydrochloride hydrate (HSCH2 CH(NH2)CO2H - xHCl - xH2O) in pure water. An ultrasonic reactor dispersed a mass of 50 mg of $Fe_3O_4$ nanoparticles in 40 mL of water for 10 min. Then, 5 mL of L-cys was added to the suspension under continuous ultrasonic treatment for 5 min. Then, the suspension was stirred mechanically for 65 h. After establishing sorption equilibrium, the particles were washed several times with distilled water, and the particles were separated after each wash with a permanent magnet. Finally, in the third step of depositing the gold shell on the $Fe_3O_4$-L-cys nanoparticles, 50 mg of $Fe_3O_4$-L-cys nanoparticles suspended in water were mixed with 40 mL of water and treated with ultrasound for 10 min. Then, this suspension was placed in the reactor with the mechanical stirrer, and every 15 min, 0.5 mL of $HAuCl_4$ solution (0.5 g $L^{-1}$) was added under stirring up. After 2h15min of stirring, the suspension was removed from the reactor and washed twice with pure water.

### 2.2. Characterization of $Fe_3O_4$@Au nanoparticles

The TEM images were realized with a Philips CM120 electron microscope (120 keV) equipped with a USC1000 SSCCD 2k x 2k Gatan camera. The hydrodynamic diameter of nanoparticles was obtained using the dynamic light scattering technique with a Malvern Zetasizer Nano ZS device.

### 2.3. Cell culture

The human lung carcinoma cells, namely A549 Dual reporter systems (NFκB and IRF) (Invivogen), are adherent epithelial cells derived from the human A549 lung carcinoma cell line. The doubling time of A549 Dual cells used was ~30h. Cells were cultured in Minimum Essential Medium (Pan biotech) supplemented with 10 % heat-inactivated fetal bovine serum (FBS, Gibco), 0.1 mg/mL penicillin-streptomycin (Pan biotech), 2 mM L-glutamine (Biochrom AG) and 0.5 μg/mL amphotericin B (Pan biotech).

### 2.4. Irradiation procedure on cells

For the irradiation experimentations, A549 Dual cells were pre-exposed to $Fe_3O_4$@Au nanoparticles for 2h before irradiation. Then, cells were irradiated with 6 megavoltage (MV) X-rays at a dose rate of 600 cGy/min with Truebeam® linear accelerator (Varian Medical Systems). Irradiations were performed at 100 cm focus to surface distance using a 15 cm × 15 cm field size at 5 cm depth with water-equivalent material. Six centimeters of water-equivalent back-scatter material was placed under the dishes containing cells, and the linear accelerator gantry was turned to an angle of 0°. Our study used different absorbed doses ranging from 0 to 8 Gy when appropriate.

### 2.5. Cell viability measurement

Human A549 Dual cells were seeded on a 96-well plate (10,000 cells/well) and allowed to grow for 24h at 37 °C/5 % $CO_2$. Then, cells were treated with increasing concentrations of $Fe_3O_4$@Au nanoparticles (ranging from 10 to 500 μg/mL) for 24–72h. Concerning the experimentations with the irradiation step, cells were exposed to 50 or 100 μg/mL $Fe_3O_4$@Au nanoparticles and irradiated with 6 MV X-rays at a dose of 6 Gy. Then, cellular viability tests were realized. Mitochondrial metabolic activity was assessed by MTT assay. Absorbance was measured using a spectrophotometer (Cytation 5 cell imaging multimode microplate, Biotech, Gen5 software) at 550–670 nm. Concerning cell counting, cells were counted using the trypan blue exclusion method.

### 2.6. Prussian blue assay

To evaluate the nanoparticles uptake by cells, A549 Dual cells were cultured on a 6-well plate (240,000 cells/well) and allowed to adhere overnight at 37 °C/5 % $CO_2$ before adding 50 or 100 μg/mL nanoparticles $Fe_3O_4$@Au for 2 or 24h. The cells were stained using the Prussian blue method, according to Khoei et al. [32]. The Prussian blue staining was observed and captured under light microscopy (Nikon microscope).

### 2.7. Measurement of survival fractions, dose enhancement factor, and mean inactivation dose

The proliferative capacity of cells following an exposition to nanoparticles combined with irradiation was evaluated by measuring the survival fraction of irradiated cells. Human A459 Dual cells were seeded in 6-well plates (180,000 cells/well) for 48h. Then, cells were exposed to 50 μg/mL or 100 μg/mL $Fe_3O_4$@Au nanoparticles and irradiated with 6 MV X-rays at different irradiation doses (0, 2, 4, 6, and 8 Gy). Cells were allowed to grow for 7 cell-division cycles, and media were replaced every 2 days. Next, cells were counted using the Trypan blue exclusion method. Surviving fractions (SF) were calculated and normalized against non-irradiated corresponding control.

The dose enhancement factor (DEF) was determined using equation (1) and according to Tabatabaie et al. [33]:

$$DEF = D_{control\ (X)}/D_{NP\ (X)} \quad (1)$$

$D_{Control\ (X)}$: The dose required to decrease in X% the viability of the cells not exposed to nanoparticles.

$D_{NP\ (X)}$: The dose required to decrease in X% the viability of the cells exposed to nanoparticles.

The area under the cell survival curve corresponding to the mean inactivation dose (MID) was determined by the Graph-Pad Prism 8 program.

### 2.8. Caspase-3/7 activity

Caspase-3/7 activity in cells exposed to nanoparticles $Fe_3O_4$@Au coupled to irradiation was determined using a Caspase-Glo assay kit (caspase-Glo® 3/7 Assays Systems, Promega). The Luminescence of each sample was read on a spectrophotometer (Cytation 5 cell imaging multimode microplate, Biotech, Gen5 software).

### 2.9. Cytotoxicity assay

Cytotoxicity was evaluated by measuring lactate dehydrogenase release (LDH) from damaged cells using a colorimetric-based kit (CytoTox 96 Non-Radioactive Cytotoxicity Assay, Promega). Cells were cultured in a 96-well plate (15,000 cells/well) for 24h, exposed to 100 μg/mL $Fe_3O_4$@Au nanoparticles, and irradiated as previously described with 6 MV X-rays at 6 Gy. Culture media were collected, and cells were lysed following the manufacturer's instructions. The absorbance was read at 490 nm on a spectrophotometer (Cytation 5 cell imaging multimode microplate, Biotech, Gen5 software). Cytotoxicity was expressed as a percent of cytotoxicity determined by the following formula (2):

$$\%\ \text{cytotoxicity} = (\text{Experimental LDH release} / \text{maximum LDH release}) \times 100 \quad (2)$$

Control refers to LDH release from untreated cells.

Double-strand DNA break staining:

Double-strand DNA breaks were quantified on A549 Dual cells exposed to nanoparticles $Fe_3O_4$@Au combined with irradiation using Gamma H2A.X Staining Kit (Abcam). Fluorescent analysis was performed using the Nikon Eclipse E2000-U microscope (Nikon), and images were obtained using the Hamamatsu ORCA-ER camera and the imaging software NIS-Element AR (Nikon).

### 2.10. Quantification of intracellular ROS levels

The intracellular ROS levels were quantified by measuring the oxidation of the fluorogenic probe 2′,7′-dichlorodihydrofluorescein diacetate (DCFH-DA) [34]. Cells were seeded in 96-well black plates (15,000 cells/well) for 48h and exposed to 100 μg/mL $Fe_3O_4$@Au nanoparticles. Plates were irradiated with 6 MV X-rays at 2 or 6 Gy doses. Then, DCF fluorescence was measured using an automated microplate reader (Cytation 5 cell imaging multimode microplate, Biotech, Gen5 software) at an excitation wavelength of 485 nm and an emission wavelength of 530 nm.

### 2.11. RT-qPCR analysis

Human A549 Dual cells were cultured in 6-well plates (240,000 cells/well) for 24h. Then, cells were exposed to 100 μg/mL $Fe_3O_4$@Au nanoparticles before being irradiated with 6 MV X-rays at a dose of 6 Gy and kept for 72 h post-irradiation before RNA extraction. Total RNA was isolated using Quick-RNA™ Viral Kit (Zymo research). The RT-qPCR was realized using the kit from Bioline with SYBR green and was carried out in QuantStudio 5 PCR thermocycler (Thermo Fisher Scientific) following a reverse transcription. The mean gene expression was reported to the GAPDH housekeeping reference gene. Moreover, absolute values were normalized

**Table 1**
Primers used for RT-qPCR analyses.

| Target gene | Forward | Reverse | Detection |
|---|---|---|---|
| Gapdh | TGCGTCGCCAGCCGAG | AGTTAAAAGCAGCCCTGGTG | Sybergreen |
| Nrf2 | GCTATGGAGACACACTACTTGG | CCAGGACTTCAGGCAATTCT | Sybergreen |
| Nox2 | GAGTTGTCACGCTGTGC | GCCCACGTACAATTCGTTCAG | Sybergreen |
| Nox4 | TCGCCAACGAAGGGGTTAAA | GACACAATCTAGCCCCAACA | Sybergreen |
| SOD1 | GTGAAGGTGTGGAGCAT | AAGTCTCCAACATGCCTCTCTT | Sybergreen |
| SOD2 | CGTTGGCCAAGGGAGATGT | GTCACGTTTGATGGCTTCCAG | Sybergreen |
| Catalase | GAATGCCCGCACCTGAGTAA | GTGCATGCAGGACAATCAGG | Sybergreen |
| GPx | CAACGTGGCCAGCTACTGAG | ACCTGGTCGGACATACTTGAGG | Sybergreen |
| IL-6 | TACAGGGAGAGGGAGCGATAA | TGGACCGAAGGCGCTTGT | Sybergreen |
| CXCL8 | CAGAGACAGCAGAGCACACA | GGCAAAACTGCACCTTCACA | Sybergreen |
| CCL2 | CTGCTCATAGCAGCCACCTT | CTTGAAGATCACAGCTTCTTTGGG | Sybergreen |
| CCL5 | TCCTCATTGCTACTGCCCTC | TCGGGTGACAAAGACGACTG | Sybergreen |
| Caspase 3 | TGGAACCAAAGATCATACATGGAA | TTCCCTGAGGTTTGCTGCAT | Sybergreen |

**CCL2 and 5:** Chemokine ligand 2 and 5; **CXCL8:** Chemokine (C-X-C motif) ligand 8; **Gapdh:** Glyceraldehyde-3-phosphate dehydrogenase; **GPx**: Glutathione peroxidase; **IL-6:** Interleukine-6; **Nox 2 and 4:** Nicotinamide adenine dinucleotide phosphate oxidase 2 and 4; **Nrf2:** Nuclear factor (erythroid-derived-2)-like 2; **SOD 1 and 2:** Superoxide dismutase Cu/Zn (1) and Mn (2).

according to the total cell number assessed by cell counting. All the primer sequences are listed in Table 1.

### 2.12. Measurements of cytokine secretion

Human A549 Dual cells were cultured in 6-well plates (240,000 cells/well) for 24h. Then, cells were exposed to 100 μg/mL $Fe_3O_4$@Au nanoparticles for 2h before being irradiated with 6 MV X-rays at a dose of 6 Gy and kept for 72h post-irradiation in the incubator. Cell culture media were collected and analyzed using a human ELISA kit to quantify the release of TNF-α, IL-1β, IL-6, CXCL8, CCL2, and CCL5 (Peprotech) according to the manufacturer's instructions. The absorbance was measured using a spectrophotometer at 450–570 nm (Cytation 5 cell imaging multimode microplate, Biotech, Gen5 software). Absolute values were normalized according to the total cell number assessed by cell counting.

### 2.13. Statistical analysis

Results were expressed as means ± standard error mean (SEM) of at least three independent cellular passages. One-way analysis of variance (ANOVA) followed by Sidak, Turkey, or Dunnett tests when appropriate were assessed. Comparison between experimental groups was performed using the GraphPad Prism 8 program (GraphPad Software, Inc.). A $p\text{-value} \leq 0.05$ was considered statistically significant.

## 3. Results

### 3.1. Characterization of $Fe_3O_4$@Au nanoparticles

The physical properties of $Fe_3O_4$@Au nanoparticles were determined using transmission electron microscopy (TEM) and the hydrodynamic size with dynamic light scattering (DLS) technique. The HRTEM image reveals monodisperse magnetite nanoparticles with an average size of 9 ± 2 nm for $Fe_3O_4$ nanoparticles and an average size of 8 ± 1 nm for $Fe_3O_4$@Au nanoparticles which is quite similar to the size of bare $Fe_3O_4$ nanoparticles (Fig. 1A–B and Table 2). Moreover, the STEM/EDX study showed a homogeneous distribution of gold, assuming a core-shell morphology of the obtained material. The hydrodynamic size measured with the DLS technique was 1895 ± 138 nm, indicating strong aggregation of bare magnetite nanoparticles. However, a substantial decrease in the hydrodynamic size of the core-shell type $Fe_3O_4$-L-cys@Au particles compared to the bare $Fe_3O_4$ nanoparticles was observed, indicating that the gold coating significantly decreased the aggregation of $Fe_3O_4$ nanoparticles.

### 3.2. Effect of $Fe_3O_4$@Au nanoparticles on A549 cell viability

To determine the dose and time-effect of $Fe_3O_4$@Au nanoparticles alone on A549 Dual cell viability, the mitochondrial metabolic activity of cells and mortality by cell counting were quantified. Results reported a significant decrease in mitochondrial metabolic activity of cells exposed to $Fe_3O_4$@Au nanoparticles at 500 μg/mL after 24, 48, and 72h of exposure (Fig. 2A). Of note, cells exposed to 200 μg/mL $Fe_3O_4$@Au nanoparticles were affected from 48h of exposure (Fig. 2B–C). The same results were observed by cell counting for $Fe_3O_4$@Au nanoparticles at 500 μg/mL (Fig. 2D–E), and a cytotoxic effect of $Fe_3O_4$@Au nanoparticles at 200 μg/mL from 72h of

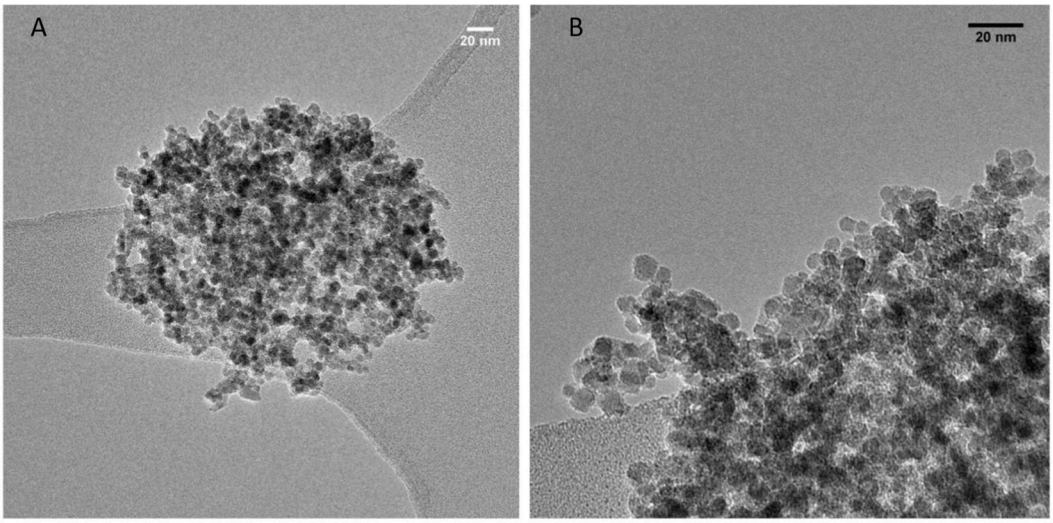


**Fig. 1.** Characterization of $Fe_3O_4$@Au nanoparticles compared to $Fe_3O_4$ nanoparticles. **(A)** High-resolution TEM images of $Fe_3O_4$ nanoparticles (10 nm scale) and **(B)** $Fe_3O_4$-L-cys@Au nanoparticles (20 nm scale) were obtained.

**Table 2**
Size of $Fe_3O_4$ and $Fe_3O_4$@Au nanoparticles.

| Nanoparticles | Hydrodynamic diameter measured by DLS (nm) | Particle Size obtained by HRTEM (nm) |
|---|---|---|
| $Fe_3O_4$ | 1895 ± 138 | 9 ± 2 |
| $Fe_3O_4$-L-cys@Au | 291 ± 40*** | 8 ± 1 |

**DLS:** Dynamic light scattering; **HRTEM:** High-resolution transmission electron microscopy. Data indicated as mean ± SEM of three independent experiments. ***: $p < 0.001$ as compared to $Fe_3O_4$ nanoparticles.

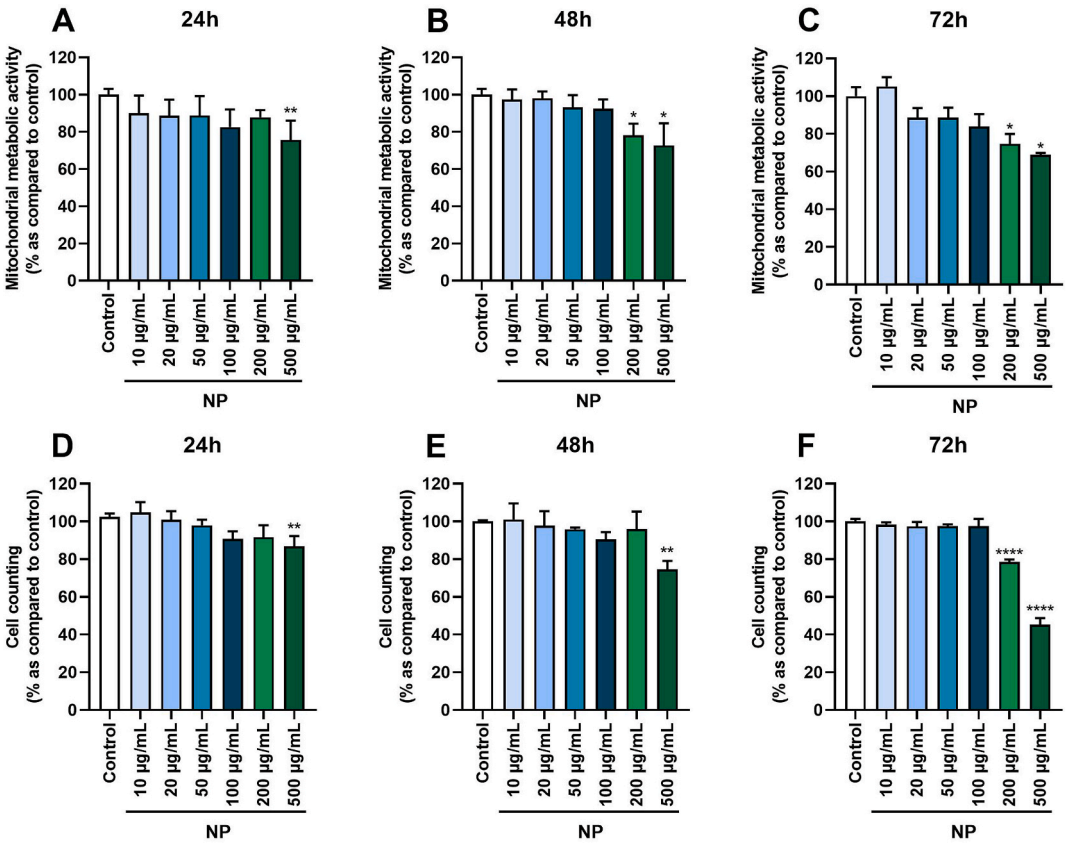


**Fig. 2.** Effect of different concentrations of $Fe_3O_4$@Au nanoparticles (NP) on A549 Dual cell viability at different times of exposure. **(A)** Mitochondrial metabolic activity of cells was measured by MTT assay after 24h, **(B)** 48h, and **(C)** 72h of exposure. **(D)** Cell counting was assessed by trypan blue exclusion method after 24h, **(E)** 48h, or **(F)** 72h of exposure. Data indicated as mean ± SEM of three independent experiments. *: $p < 0.05$; **: $p < 0.01$ and ****: $p < 0.0001$ as compared to control condition.

exposure was noted (Fig. 2F). None of the other concentrations of $Fe_3O_4$@Au nanoparticles tested altered the mitochondrial metabolic activity or cell viability. According to these results, concentrations of 50 and 100 µg/mL of $Fe_3O_4$@Au nanoparticles were thus selected to investigate the effect of nanoparticles effect coupled to irradiation.

### *3.3. Uptake of $Fe_3O_4$@Au nanoparticles by A549 cells*

Next, the ability of nanoparticles to cross the membrane and accumulate in cells was evaluated. The Prussian blue staining was performed after 2 and 24h of exposure to 50 and 100 µg/mL nanoparticles and followed by multiple washes to eliminate excess nanoparticles. As shown in Fig. 3 obtained by optical microscopy, the blue staining demonstrated an intracellular accumulation of nanoparticles compared to the control condition. After 2h of exposure to 50 µg/mL (Fig. 3B) or 100 µg/mL nanoparticles (Fig. 3C), an increased blue staining compared to the control condition (Fig. 3A) was noted, as well as after 24h of exposure to 50 µg/mL (Fig. 3E) and 100 µg/mL nanoparticles (Fig. 3F) compared to corresponding control (Fig. 3D). Interestingly, the cellular uptake of nanoparticles increased with the nanoparticle concentrations.

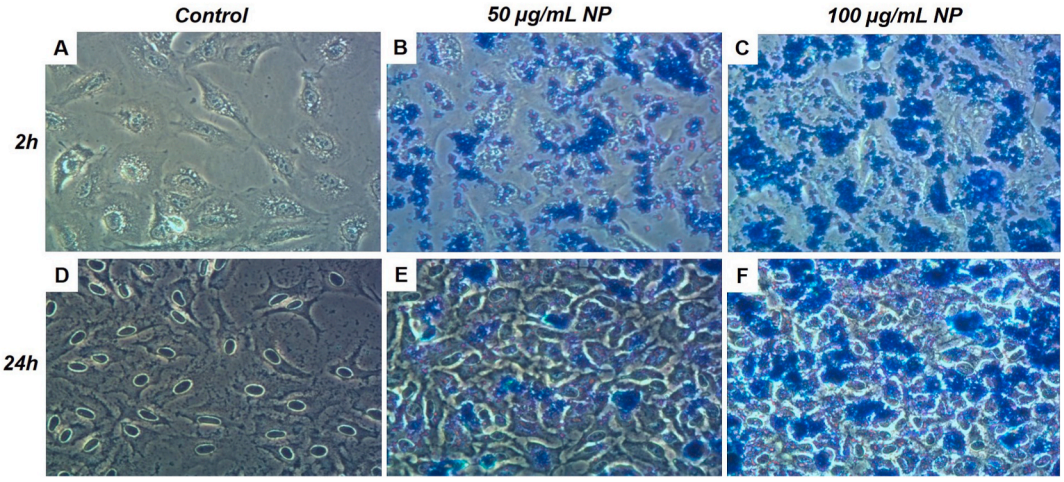


**Fig. 3.** Detection of intracellular $Fe_3O_4$@Au nanoparticle levels (NP) on A549 Dual cells. The uptake was assessed by Prussian blue staining. **(A)** Control condition, **(B)** 50 µg/mL $Fe_3O_4$@Au nanoparticles condition, and **(C)** 100 µg/mL $Fe_3O_4$@Au nanoparticles condition were evaluated after 2h of exposure. **(D)** The control condition, **(E)** 50 µg/mL $Fe_3O_4$@Au nanoparticles condition, and **(F)** 100 µg/mL $Fe_3O_4$@Au nanoparticles condition were also tested after 24h of exposure. Blue staining indicates intracellular uptake of $Fe_3O_4$@Au nanoparticles.

### *3.4. Effect of $Fe_3O_4$@Au nanoparticles combined with irradiation on A549 cell viability*

In a new set of experiments, the effect of $Fe_3O_4$@Au nanoparticles combined with or without irradiation was evaluated on cellular viability. As shown in Fig. 4, no significant effect was noted on the mitochondrial metabolic activity of A549 Dual cells non-irradiated and exposed to 50 or 100 µg/mL $Fe_3O_4$@Au nanoparticles for 24h (Fig. 4A), 48h (Fig. 4B) or 72h (Fig. 4C) as previously shown for Fig. 2. Interestingly, with irradiation alone, the mitochondrial metabolic activity was significantly decreased at 48h and 72h (but not at 24h) compared to non-irradiated control conditions. Moreover, when both treatments were applied, our results indicated no potentiation of irradiation by nanoparticles, whatever the nanoparticle concentrations used.

Concerning cell counting results, no modulation of the viability of non-irradiated cells after 24h (Fig. 4D), 48h (Fig. 4E), and 72h (Fig. 4F) of exposure to both studied nanoparticle concentrations was detected. As demonstrated by mitochondrial metabolic activity results, after 24 and 48h of exposure to nanoparticles combined with irradiation, the viability of irradiated cells was affected compared to non-irradiated control. Still, potentiation of irradiation by nanoparticles was observed. However, 72h post-irradiation, results showed a significant decrease in the cell count of irradiated cells compared to the non-irradiated control condition and a reduction of cellular viability of irradiated cells exposed to nanoparticles compared to the irradiated control condition. Consistent with these results, all subsequent experiments were performed at 72h post-6 Gy irradiation.

### *3.5. Effect of $Fe_3O_4$@Au nanoparticles combined with irradiation on the proliferative capacity of A549 cells*

The survival fractions after irradiation were measured to determine the effect of $Fe_3O_4$@Au nanoparticles combined with irradiation and the dose effect of irradiation on the survival of A549 Dual cells (Fig. 5).

The survival fractions decreased with increasing doses of irradiation. At 2 Gy irradiation, no difference in survival fractions with or without $Fe_3O_4$@Au nanoparticles were observed. At 4 Gy irradiation, a significant decrease in cell survival of A549 Dual cells incubated with 50 and 100 µg/mL of $Fe_3O_4$@Au nanoparticles compared to control conditions without nanoparticles was noticed. At 6 and 8 Gy irradiation doses, a decrease in survival fraction was also noted, but only for 100 µg/mL nanoparticles at 6 Gy irradiation. Importantly, no difference was observed between the MID of cells exposed to nanoparticles and control cells without nanoparticles (Table 3). However, only 100 µg/mL nanoparticles significantly potentiated the irradiation at specific doses of 4, 6, and 8 Gy.

Next, the DEF obtained from the cell survival curves was used to determine the effects of $Fe_3O_4$@Au nanoparticles as a dose enhancer on the A549 cell line (Table 4). A549 cells exhibited a $DEF_{(80)}$ of 1.16 in the presence of nanoparticles. Interestingly, 50 and 100 µg/mL nanoparticles enhanced by about 16 % the radiobiological effects of IR on cells. According to the aforementioned results, 100 µg/mL $Fe_3O_4$@Au nanoparticle concentration was selected for the following experiments.

### *3.6. Effect of $Fe_3O_4$@Au nanoparticles combined with irradiation on A549 cells apoptosis, necrosis, and double-strand DNA breaks*

To evaluate the gene expression as well as the activity of apoptosis and necrosis markers 72h post-irradiation, the expression of mRNA of caspase-3 (Fig. 6A), the biological activity of caspase-3/7 (Fig. 6B) and LDH release (Fig. 6C) were measured.

Results at 72h showed that the expression of caspase-3 mRNA was upregulated by irradiation but not by nanoparticle when used alone compared to untreated control. Moreover, nanoparticles combined with irradiation significantly further upregulated caspase-3 gene expression in cells. The same results were observed concerning caspase-3/7 activity and LDH levels, which were significantly

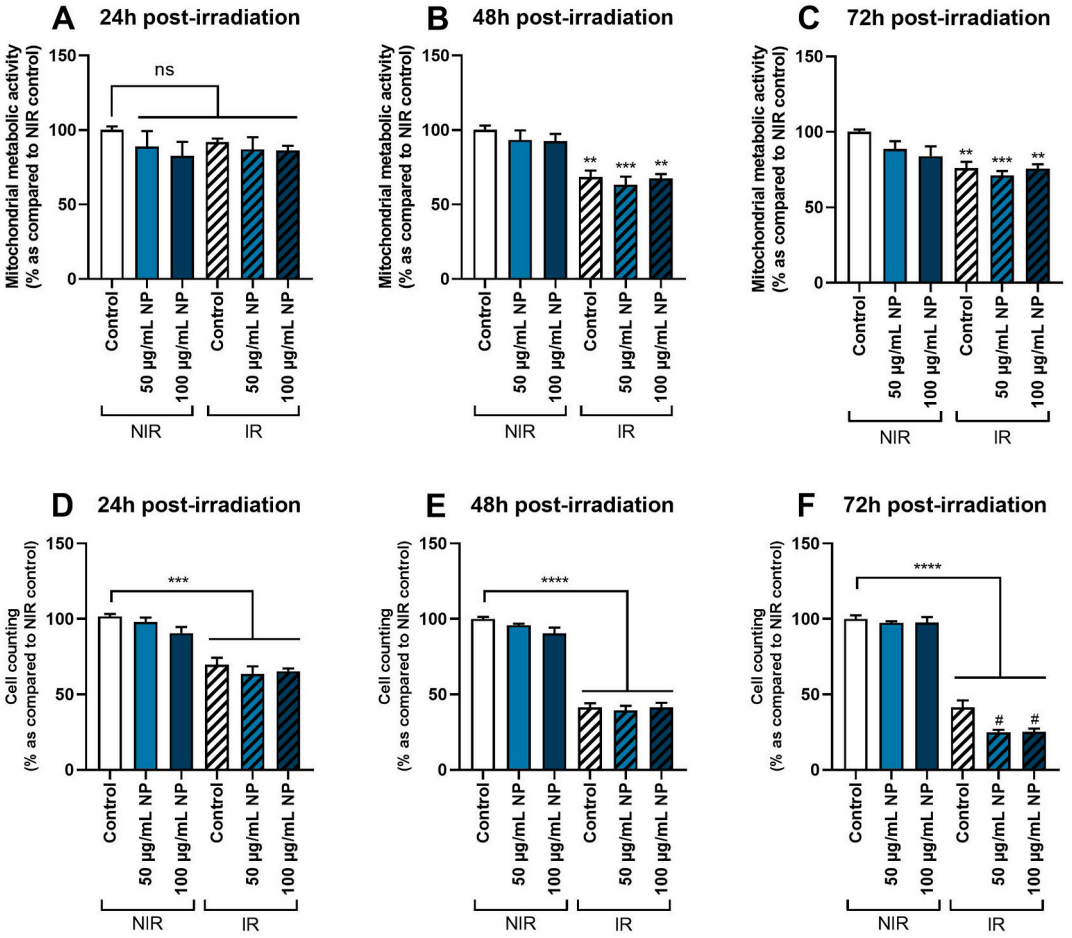


**Fig. 4.** Effect of different concentrations of $Fe_3O_4$@Au nanoparticles (NP) combined with 6 Gy irradiation on A549 Dual cell viability at different times of exposure. **(A)** Mitochondrial metabolic activity of non-irradiated (NIR) and irradiated (IR) cells was performed by MTT assay 24h, **(B)** 48h, and **(C)** 72h post-irradiation. **(D)** Cell counting on IR and NIR cells was assessed by trypan blue exclusion method 24h, **(E)** 48h, or **(F)** 72h post-irradiation. Data indicated as mean ± SEM of three independent experiments. **: $p < 0.01$; ***: $p < 0.001$ and ****: $p < 0.0001$ as compared to non-irradiated control condition. #: $p < 0.05$ as compared to the irradiated control condition.

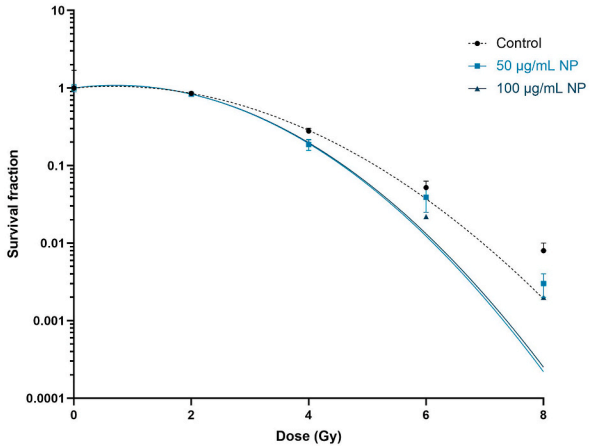


**Fig. 5.** Effect of $Fe_3O_4$@Au nanoparticles (NP) at 50 and 100 µg/mL on the proliferative capacity of A549 Dual cells irradiated at different irradiation doses. The survival fraction was obtained by cell counting after *7* cell-division cycles post-irradiation. Data indicated as mean ± SEM of three independent experiments. *: $p < 0.05$ and **: $p < 0.01$ as compared to the control condition at the same irradiation dose as nanoparticle conditions.

**Table 3**
Determination of survival fraction and mean inactivation dose in the presence of nanoparticles and treated by 6 MV photon beam irradiation.

| | Dose (Gy) | Control | 50 μg/mL NP | 100 μg/mL NP |
|---|---|---|---|---|
| Survival fraction | 0 | 1.00 ± 0.069 | 1.00 ± 0.110 | 1.00 ± 0.030 |
| | 2 | 0.853 ± 0.018 | 0.833 ± 0.027 | 0.883 ± 0.031 |
| | 4 | 0.278 ± 0.025 | 0.187 ± 0.030** | 0.195 ± 0.019** |
| | 6 | 0.052 ± 0.011 | 0.039 ± 0.014 | 0.022 ± 0.001** |
| | 8 | 0.008 ± 0.002 | 0.003 ± 0.001* | 0.002 ± 0.000* |
| MID | – | 3.37 ± 0.10 | 3.12 ± 0.13 | 3.20 ± 0.07 |

**MID:** Mean inactivated dose; **NP:** Nanoparticles.
Survival fraction and MID were obtained from the survival curve of cells exposed or not to 50 or 100 μg/mL nanoparticles and cells irradiated at different irradiation doses. Data indicated as mean ± SEM of three independent experiments. *: $p < 0.05$ and **: $p < 0.01$ as compared to the control condition at the same irradiation dose as nanoparticle conditions.

**Table 4**
Dose enhancement factor for $Fe_3O_4$@Au nanoparticles.

| | Control | 50 μg/mL NP | 100 μg/mL NP |
|---|---|---|---|
| $DEF_{(50)}$ | 1.00 ± 0.02 | 1.07 ± 0.02 | 1.07 ± 0.03 |
| $DEF_{(80)}$ | 1.00 ± 0.04 | 1.16 ± 0.04* | 1.16 ± 0.03* |

**DEF:** Dose enhancement factor; **NP:** Nanoparticles.
DEF values were obtained from the survival curve of cells exposed or not to 50 or 100 μg/mL nanoparticles and calculated for 50 and 80 % of cell death. Data indicated as mean ± SEM of three independent experiments. *: $p < 0.05$ as compared to the DEF of the control condition.

elevated on cells exposed to 100 μg/mL of $Fe_3O_4$@Au nanoparticles coupled to 6 Gy irradiation. Nanoparticles potentiated irradiation deleterious effect, leading to cell death by apoptosis. Irradiation may also cause single and double-strand DNA breaks, promoting cancerous cell death. To observe if $Fe_3O_4$@Au nanoparticles combined with irradiation could increase the level of DNA breaks in cells, immunostaining a DNA damage marker, namely phosphorylated Gamma H2A.X histone, was performed [35]. Results also reported that control and $Fe_3O_4$@Au nanoparticles alone did not induce double-strand DNA breaks in cells (Fig. 6D). However, after the irradiation, an increase in the level of DNA damage in the cells was observed. Etoposide was used herein as the positive control. Interestingly, $Fe_3O_4$@Au nanoparticles combined with irradiation induced a modest level of double-strand DNA breaks compared to irradiation alone.

### *3.7. Effect of $Fe_3O_4$@Au nanoparticles combined with irradiation at 2 or 6 Gy on ROS production by A549 dual cells*

To explore the effect of $Fe_3O_4$@Au nanoparticles combined with irradiation and the dose effect of irradiation on the redox status of A549 Dual cells, intracellular ROS levels were measured using a DCFH-DA probe. Interestingly, data demonstrated that irradiation at 2 Gy (Fig. 7A) or 6 Gy (Fig. 7B) significantly increased the intracellular ROS level compared to the non-irradiated control condition. The ROS production was significantly elevated after incubation with 100 μg/mL $Fe_3O_4$@Au nanoparticles without irradiation, and nanoparticles-induced ROS production was potentiated after 2 or 6 Gy irradiation. Concerning the dose-effect of irradiation on ROS production, a dose-effect of irradiation on redox status with a significant elevation of ROS production was noted after a 6 Gy irradiation compared to cells exposed to 2 Gy irradiation (Fig. 7C).

### *3.8. Effect of $Fe_3O_4$@Au nanoparticles combined with 6 Gy irradiation on the expression of genes encoding redox markers on A549 cells*

Then, the expression of genes encoding ROS-producing enzymes, namely, NADPH oxidase 2 (Nox2) and 4 (Nox4), was evaluated. Results demonstrated that $Fe_3O_4$@Au nanoparticles did not modulate the expression of genes encoding Nox2 (Fig. 8A) and Nox4 (Fig. 8B) without irradiation. Interestingly, 6 Gy irradiation promoted upregulation of the expression of genes encoding Nox2 and Nox4 compared to the non-irradiated control condition. Moreover, concerning Nox2 gene expression, data showed that 100 μg/mL $Fe_3O_4$@Au nanoparticles significantly potentiated the upregulation induced by 6 Gy irradiation on A549. Then, the expression of genes encoding major enzymes of the antioxidant defense system was evaluated. Results demonstrated that without irradiation, nanoparticles did not regulate the expression of genes encoding SOD1 (Fig. 8C), SOD2 (Fig. 8D), catalase (Fig. 8E), GPx (Fig. 8F) and the redox-dependent transcription factor Nrf2 (Fig. 8G). However, after irradiation, a significant upregulation of genes encoding all enzymes of the antioxidant defense system and the redox transcription factor Nrf2 compared to the non-irradiated control condition was observed. Notably, except for GPx, $Fe_3O_4$@Au nanoparticles significantly potentiated the upregulation induced by 6 Gy irradiation on cells with an increase in mean gene expressions of antioxidant markers of cells exposed to nanoparticles and irradiated.

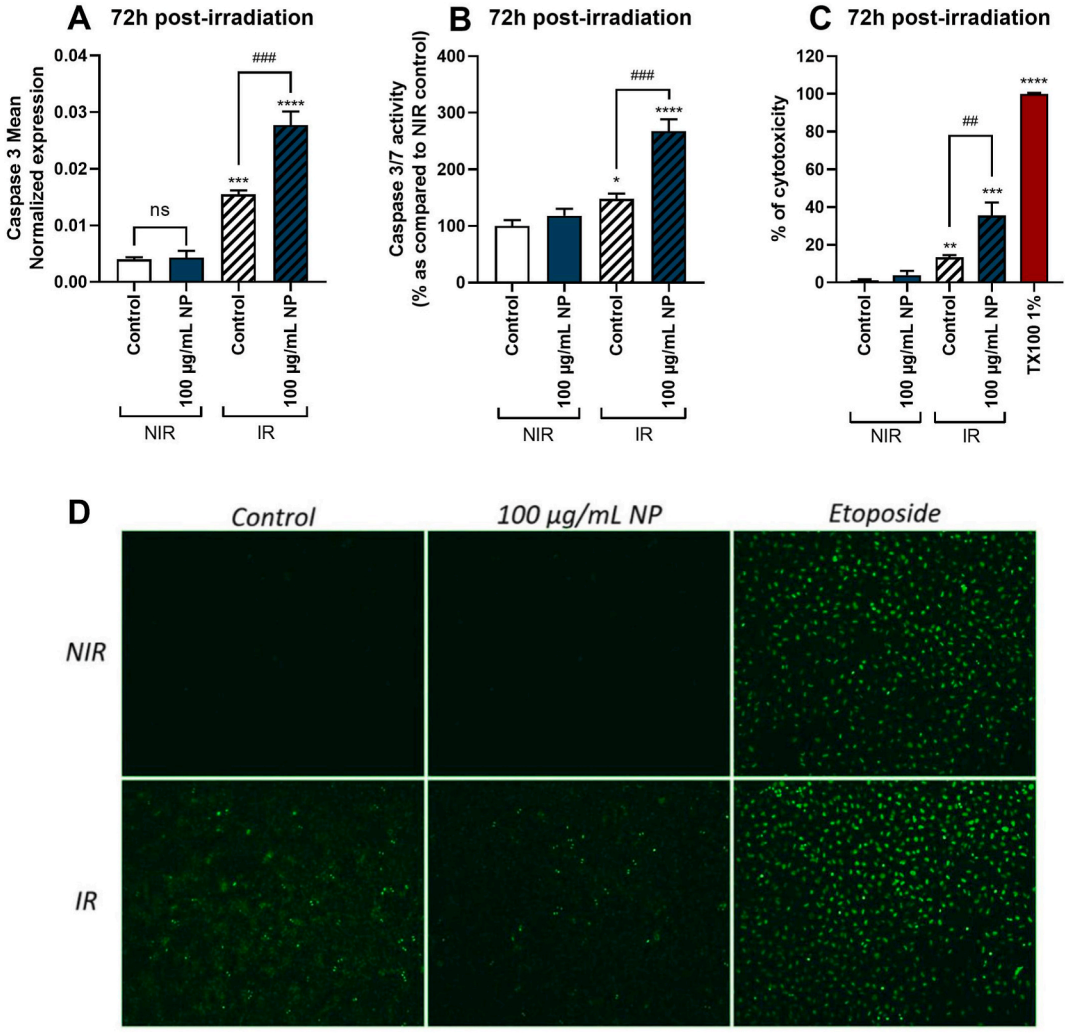


**Fig. 6.** Effect of $Fe_3O_4$@Au nanoparticles (NP) combined with 6 Gy irradiation on A549 Dual cell viability, 72h post-irradiation and on DNA double-strand breaks, 0.5h post-irradiation. **(A)** The mean expression of gene encoding caspase 3 was obtained by RT-qPCR on non-irradiated (NIR) and irradiated (IR) cells. **(B)** Caspase 3/7 activity of NIR and IR cells was performed by Caspase-Glo assay 72h post-irradiation. **(C)** LDH release of NIR and IR cells was performed by LDH assay 72h post-irradiation. **(D)** The level of DNA damage was measured by immunolabeling phosphorylated gamma H2A.X histone of NIR and IR cells 0.5h post-irradiation. Data indicated as mean ± SEM of three independent experiments. *: $p < 0.05$; **: $p < 0.01$; ***: $p < 0.001$ and ****: $p < 0.0001$ as compared to non-irradiated control condition. ##: $p < 0.01$; ###: $p < 0.001$ as compared to irradiated control condition. The immunostaining was analyzed by fluorescence microscopy.

### *3.9. Effect of $Fe_3O_4$@Au nanoparticles combined with 6 Gy irradiation on gene expression and production of pro-inflammatory markers on A549 cells*

The immune system plays a critical role in controlling the establishment and spread of cancer. Then, the effect of $Fe_3O_4$@Au nanoparticles combined with 6 Gy irradiation on the cell pro-inflammatory response was explored, and firstly, the expression of genes coding for major pro-inflammatory cytokines and chemokines.

As shown in Fig. 8, irradiation of cells exposed or not to nanoparticles induced a significant upregulation of genes encoding IL-6 (Fig. 9A), CXCL8 (Fig. 9B), CCL2 (Fig. 9C) and CCL5 (Fig. 9D). Of note, only the expression of the gene coding for CCL2 was down-regulated by the exposition to nanoparticles without irradiation, whereas nanoparticles modulated no other gene expressions without irradiation. No potentiation of irradiation by nanoparticles for IL-6, CCL2, and CCL5 gene expressions was reported. Interestingly, the expression of the gene encoding CXCL8 was significantly upregulated on cells exposed to nanoparticles and irradiated compared to the irradiated control condition.

Secondly, the protein levels of pro-inflammatory cytokines and chemokines, namely, TNF-α, IL-1β, IL-6, CXCL8, CCL2, and CCL5, were quantified in the cells incubated or not with 100 µg/mL $Fe_3O_4$@Au nanoparticles and irradiated. The $Fe_3O_4$@Au nanoparticles without irradiation did not induce modulation of TNF-α (Fig. 9E), IL-1β (Fig. 9F), IL-6 (Fig. 9G), CXCL8 (Fig. 9H), CCL2 (Fig. 9I) and

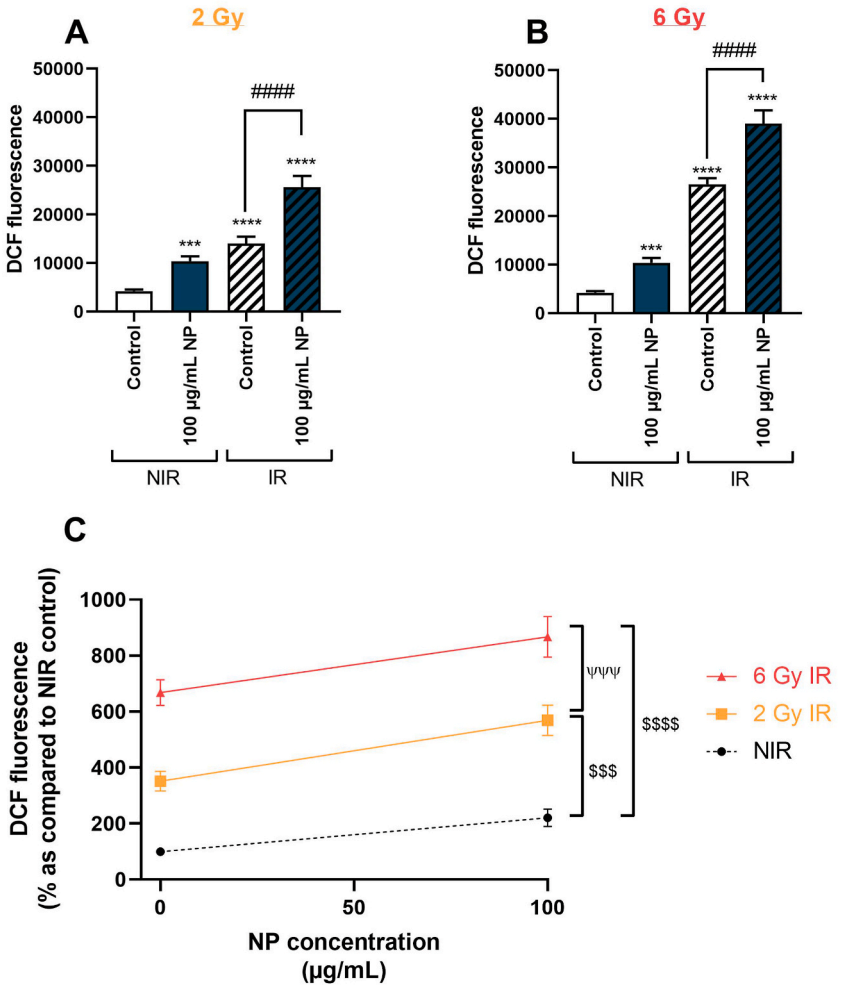


**Fig. 7.** Effect of $Fe_3O_4$@Au nanoparticles (NP) combined with 2 or 6 Gy irradiation on ROS production by A549 Dual cells. **(A)** ROS production of non-irradiated (NIR) or irradiated (IR) cells at 2 Gy irradiation dose or **(B)** at 6 Gy irradiation dose and **(C)** the effect of $Fe_3O_4$@Au nanoparticles on the ROS levels after 0, 2, or 6 Gy irradiation were determined. The ROS production was measured using a DCFH-DA probe. Data are shown as mean ± SEM of three independent experiments. ***: $p < 0.001$ and ****: $p < 0.0001$ as compared to non-irradiated control condition. ####: $p < 0.0001$ as compared to the irradiated control condition. $$$: $p < 0.001$ and $$$$: $p < 0.0001$ as compared to the AUC of the non-irradiated curve and ψψψ: $p < 0.001$ as compared to the AUC of the 6 Gy irradiation curve.

CCL5 (Fig. 9J) secretion compared to non-irradiated control condition 72h post-irradiation. Furthermore, irradiation significantly elevated cytokine and chemokine releases compared to non-irradiated control conditions with or without nanoparticles. However, results reported an increase in the cytokines and chemokines secreted, except for CCL2, in cells exposed to nanoparticles combined with irradiation compared to the irradiated control condition.

## 4. Discussion

Cancer represents a leading cause of death worldwide and always challenges medical research to find new effective approaches to improve the prevention, diagnosis, monitoring, and treatment of all cancer types. Thus, cancer drives an expansion of related research and biomedical progress. With a predicted compound annual growth rate of 17 % for solid cancers and 10 % for hematological cancers between 2023 and 2027, the global spending on cancer medicines could reach US$375 Billion by 2027 [2,36].

Nanomedicine, and particularly theragnostic nanomaterials, developed for cancer treatment in more than 50 % of cases, offer promising outlooks for their radiosensitizing properties or as vehicles for therapeutic agents [36–38].

However, nanoparticles also present disadvantages, such as instability, toxicity, lack of biocompatibility, poor targeting specificity, production cost, and related environmental and health issues to their production, which limit their acceptability, creating a gap between theoretical predictions and commercial viability [39]. Otherwise, the global market size of metallic nanoparticles was USD 2.4 billion in 2021 [40].

Thus, one of the challenges concerning nanotechnology, such as nanoparticles, is the interactions with cells and tissues. These

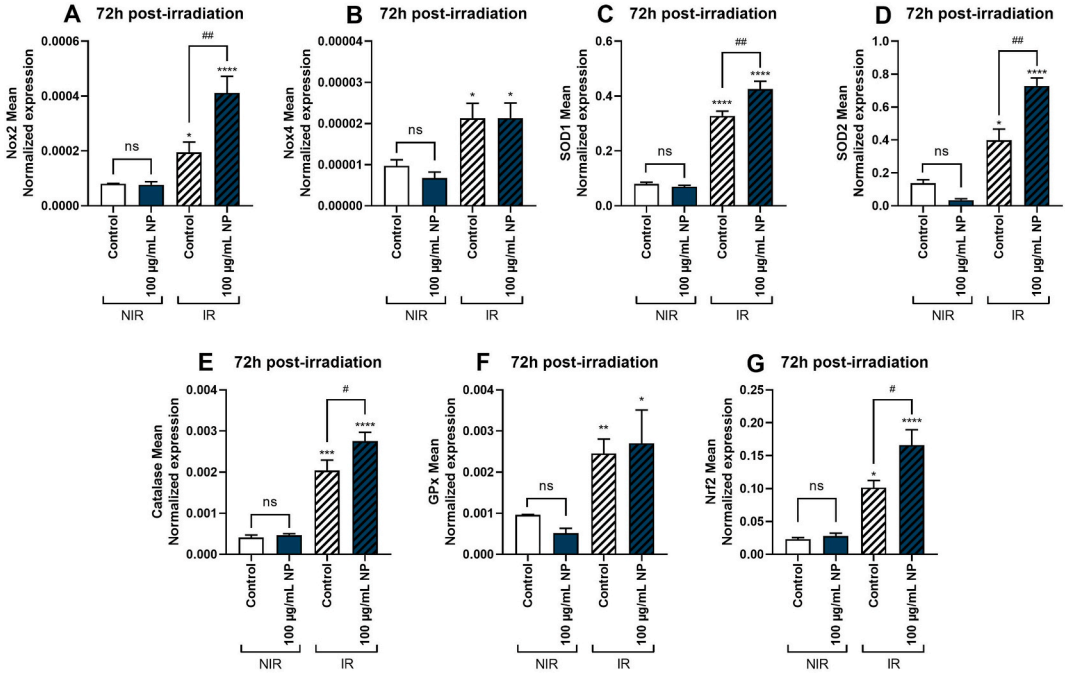


**Fig. 8.** Effect of $Fe_3O_4$@Au nanoparticles (NP) combined with 6 Gy irradiation on expression of genes encoding redox markers of A549 Dual cells, 72h post-irradiation. The mean expression of genes coding for redox markers was obtained by RT-qPCR on non-irradiated (NIR) and irradiated (IR) cells. Expression of genes encoding **(A)** Nox 2, **(B)** Nox 4, **(C)** SOD1, **(D)** SOD2, **(E)** catalase, **(F)** GPx, and **(G)** Nrf2 were determined 72h post-6 Gy irradiation. All data were normalized by cell counting. Data expressed as mean ± SEM of three independent experiments. *: $p < 0.05$; **: $p < 0.01$; ***: $p < 0.001$; ****: $p < 0.0001$ as compared to non-irradiated control condition. #: $p < 0.05$; ##: $p < 0.01$ as compared to irradiated control condition.

interactions can modify the biological properties of nanoparticles, decrease their stability, alter their biocompatibility leading to render them ineffective for regulating the proliferation of cancer cells or induce unintended harm [30]. The shape, size, composition (core and coating), ligands, and nanoparticle charge are crucial for NPs-associated toxicity [24,36,41]. Moreover, the synthetic process chosen for nanoparticles is crucial due to the cost and environmental concerns around nanomaterials production.

In this article, the ability of a new type of nanoparticle, a hybrid core-shell magnetite coated with gold: $Fe_3O_4$@Au, to potentiate the deleterious effect of ionizing radiation on an *in vitro* model of lung cancer cells was evaluated by focusing on the oxidative stress and pro-inflammatory response of cells leading to cell death. The nanoparticles studied were produced following principles of green synthesis using the sonochemistry method [31].

The sonochemistry is used as a green method for nanoparticle preparation. It notably involves using fewer toxic compounds and environmentally safe solvents while improving reaction conditions and selectivity. Indeed, it has been demonstrated on core−shell $Fe_3O_4$@$SiO_2$ that sonochemistry permitted an increased magnetization value and a decrease in magnetite oxidation owing to the high speed of sonochemical coating [31].

$Fe_3O_4$ NPs have been extensively studied among metallic nanoparticles exhibiting therapeutic effects due to their biocompatibility, stability, prolonged *in vivo* circulation time, or high self-metabolism [42]. However, $Fe_3O_4$ NPs also show toxic effects on cells by necrosis and apoptosis processes [24]. It has been demonstrated that $Fe_3O_4$ NPs exhibited strong susceptibility to acid and oxidation degradation associated with a high degree of agglomeration, as observed in Table 2. This agglomeration is due to their strong magnetic attractions and van der Waals interactions between particles [3,43].

The interest in using hybrid nanoparticles is that coating organic/inorganic compounds with noble metals enhances stability, biocompatibility and toxicity [44,45]. The core-shell $Fe_3O_4$@Au NPs have unique physicochemical properties. The superparamagnetism is provided by $Fe_3O_4$ particles and the gold shell provides superior optical properties, decreases toxicity and improves biocompatibility, stability, catalytic activity, and surface functionality [26,27,46]. The size of core-shell $Fe_3O_4$@Au nanoparticles is illustrated in Fig. 1 and reported in Table 2, as well as the anti-aggregation role of the gold coating that is known to improve the functionality and stability of nanoparticles and limit $Fe_3O_4$-induced apoptosis [47].

First, the cellular uptake of studied hybrid nanoparticles was demonstrated in Fig. 3 of the present work. Literature data reported a time-dependent intracellular uptake of $Fe_3O_4$@Au NPs on a breast cancer cell line as well as the role of lysosomes mediated by clathrins, in the endocytosis process [48,49]. Our study noted a cytotoxic concentration of 200 µg/mL $Fe_3O_4$@Au NPs (Fig. 2). AuNPs and $Fe_3O_4$NPs are biologically non-inert and could promote cell death in a concentration and time-dependent manner on lung carcinoma and breast cancer cells [50,51]. The involved mechanisms are apoptosis, necrosis, autophagy, or a loss of redox homeostasis, leading to apoptosis and necrosis [51,52].

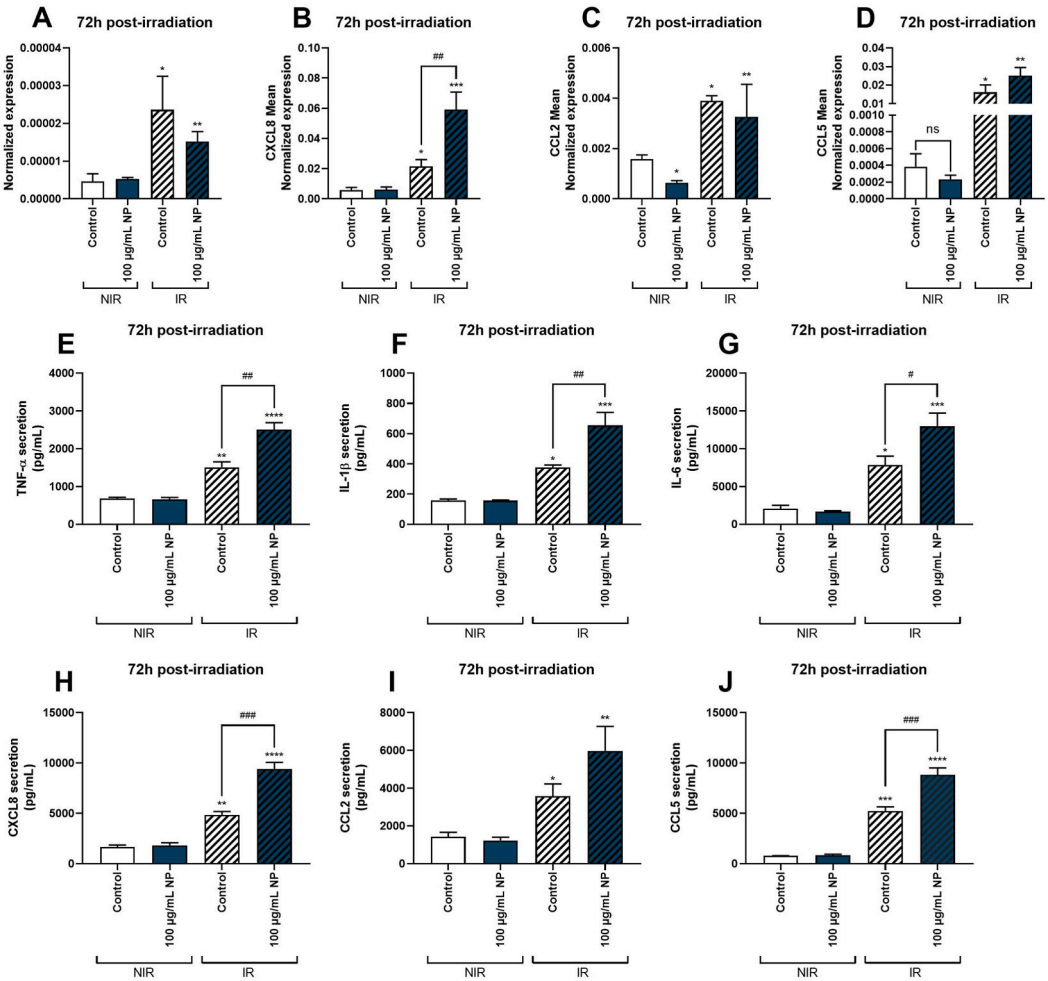


**Fig. 9.** Effect of $Fe_3O_4$@Au nanoparticles (NP) combined with 6 Gy irradiation on expression of genes encoding pro-inflammatory markers of A549 Dual cells, 72h post-irradiation. Mean expression of genes coding for pro-inflammatory markers was obtained by RT-qPCR on non-irradiated (NIR) and irradiated (IR) cells. Expression of genes encoding **(A)** IL-6, **(B)** CXCL8, **(C)** CCL2, and **(D)** CCL5 were determined 72h post-6 Gy irradiation. The pro-inflammatory response was also quantified by measuring secreted levels of **(E)** TNF-α, **(F)** IL-1β, **(G)** IL-6, **(H)** CXCL8, **(I)** CCL2 and **(J)** CCL5 72h post-irradiation by ELISA. All data were normalized by cell counting. Data indicated as mean ± SEM of three independent experiments. *: $p < 0.05$; **: $p < 0.01$; ***: $p < 0.001$ ****: $p < 0.0001$ as compared to non-irradiated control condition; ##: $p < 0.01$ as compared to irradiated control condition.

The potentiation of irradiation by hybrid nanoparticles was demonstrated on cell viability, according to Butterworth et al., particularly for megavolt irradiations [53]. Ionizing radiation used in radiotherapy interacts with high-atomic number atoms in the nanoparticles and causes physical, chemical, and biological additional reactions that will increase tumor cell damage [32,54,55]. $Fe_3O_4$@Au nanoparticles potentiate ionizing radiation effects on cell proliferation and activation of apoptosis and necrosis (Figs. 4–6). Multiple *in vivo* studies reported that metallic nanoparticles coupled to irradiation on tumor models induced an activation of caspase 3 and an inhibition of survival and proliferation signaling markers such as mitogen-activated protein kinase signaling pathways [56,57]. Most studies exposing the clinical potential of metallic nanoparticles in combination with radiotherapy explained that nanoparticles act as radiosensitizers by causing a ROS elevation associated with a redox imbalance, leading to cell death depending on nanoparticle size, shape, and surface charge [58–61]. Significantly, as shown in Figs. 7 and 8, $Fe_3O_4$@Au nanoparticles coupled with irradiation promoted a redox imbalance in a radiation dose-dependent manner. $Fe_3O_4$ nanoparticles can catalyze the generation of free radicals by the Fenton and Haber-Weiss reactions and lead to hydroxyl radical generation [21,62]. Ionizing radiation interacts with high-atomic number atoms in the nanoparticles, generating secondary photoelectrons or Auger electrons, which promote the production of ROS [63,64].

In the present work, $Fe_3O_4$@Au nanoparticles did not induce an elevation of double-strand DNA breaks coupled or not to irradiation (Fig. 6). However, $Fe_3O_4$@Au nanoparticles exhibit high-Z atoms and interact with ionizing radiation, leading to amplify the energy deposited in tumor tissues, and cells and to promote increased tumor cell death through an indirect mechanism involving oxidative stress and pro-inflammatory response [18,51,65]. The modelization of cell response helping to predict the deleterious effect

of nanoparticles coupled with irradiation on cells was always "underrated" because of the biological response and the redox signaling pathways constitutively activated after irradiation [53].

Interestingly, the present study reported an important dysregulation of redox markers associated with a pro-inflammatory response on cells incubated with nanoparticles before being irradiated (Figs. 8 and 9). However, not all the markers were dysregulated, suggesting that irradiation coupled with nanoparticles activates preferential signaling pathways. Radiotherapy caused a pro-inflammatory state through an important secretion of cytokines and chemokines to activate the immune system and recruit immune cells into the tumor microenvironment [65,66]. In the present study, the pro-inflammatory response could also be relative to necrosis and apoptosis activations induced by high-dose radiotherapy and potentiated by nanoparticles. These nanoparticles give a supplementary synergic effect to the tumoricidal effect of irradiation.

For this beam energy, the main interactions are Compton scattering and pair production. For materials with a high Z, such as iron (Z = 26), it has been shown that the predominant interaction at 6 MV is Compton scattering [67,68]. Also, as shown in Table 4, the significant increase in the $DEF_{(80)}$ demonstrated an interest in continuing the investigations on this new type of nanoparticles. A potentiation of 16 % would significantly reduce the side effects of radiotherapy treatment and provide a better control of the disease.

Metallic nanoparticles, in combination with radiotherapy, have displayed promising potential. However, it appears crucial to identify an optimal care protocol where nanoparticles could be provided a benefit. The radiation potentiated by metallic nanoparticles such as $Fe_3O_4$@Au nanoparticles could be considered in inoperable, localized, and non-metastatic tumors. Indeed, radiotherapy protocols adjuvant to chemotherapy are already robust for metastatic tumors. On the other hand, in cases of single radiotherapy treatment, using a radiosensitizer could improve the clinical results.

To conclude, the present study showed that $Fe_3O_4$@Au nanoparticles synthesized by a green method, namely sonochemical approach, have been internalized in carcinoma lung cells. Moreover, the potential of $Fe_3O_4$@Au nanoparticles to enhance the radiosensitivity of lung carcinoma epithelial cells through a significant dysregulation of redox and inflammatory status, causing the alteration of the proliferative capacity of cancerous cells, apoptosis, and necrosis, has been demonstrated (Fig. 10). This hybrid nanoparticle of a magnetite core embedded in a gold shell exhibits radiosensitizing effects and could be combined with radiotherapy

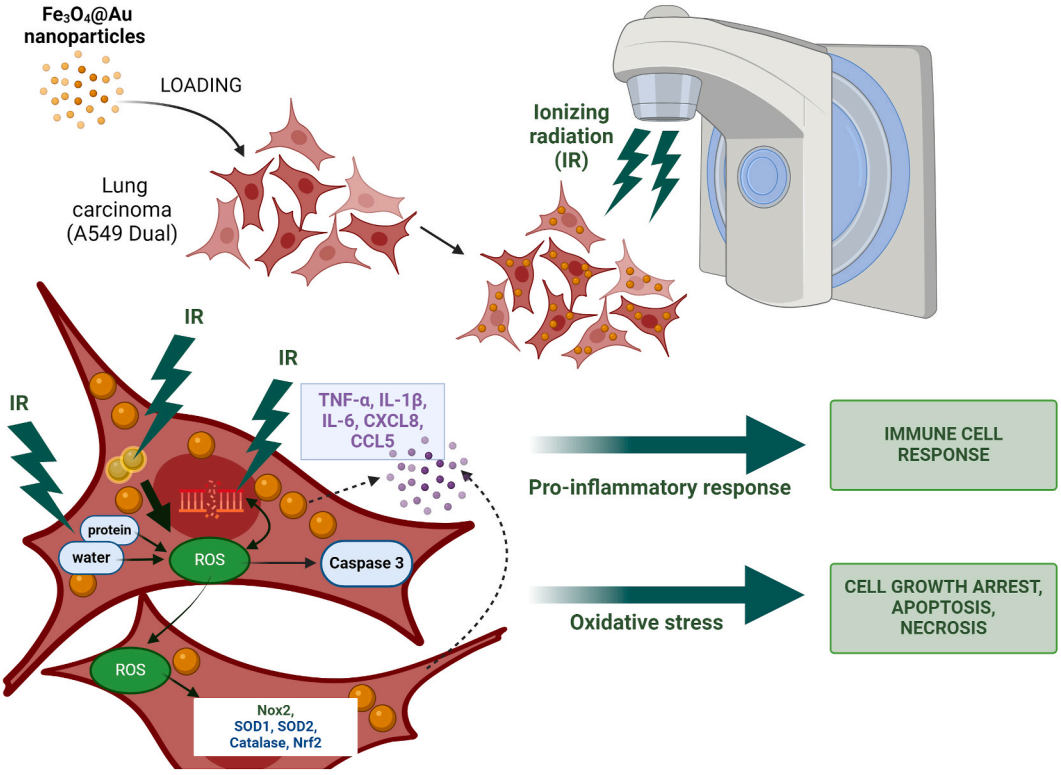


**Fig. 10.** Overview of the mechanisms induced by $Fe_3O_4$@Au nanoparticles coupled to irradiation in tumor cells. The irradiation causes oxidative stress on the lung carcinoma epithelial cells by increasing ROS levels, up-regulating ROS-producing enzyme gene expressions, and over-activating the antioxidant defense system. Importantly, once internalized within cell cytosol, $Fe_3O_4$@Au nanoparticles act as radiosensitizers by potentiating the deleterious effect of a 6 Gy irradiation dose. $Fe_3O_4$@Au nanoparticles combined with irradiation increase ROS levels, the gene expression of redox markers such as Nox2, antioxidant enzymes namely SOD1, SOD2, catalase, and the redox-dependent transcription factor Nrf2. On the other hand, the loss of redox homeostasis induced by irradiation leads to a pro-inflammatory response. This pro-inflammatory response is potentiated by the nanoparticles coupled with irradiation, promoting an overproduction of cytokines and chemokines, namely TNF-α, IL-1β, IL-6, CXCL8, and CCL5. Finally, these dysregulations alter cellular proliferation and amplify apoptosis and necrosis of tumor cells exposed to $Fe_3O_4$@Au nanoparticles combined with irradiation.

against radioresistant cancer. Importantly, architecting core-shell nanosystems considerably helps improve the stability and biocompatibility of nanoparticles. For metal nanoparticles evaluated in this work, the $Fe_3O_4$ core associated with gold shell confers to these hybrid nanoparticles' radiosensitizing potential and their ability to be internalized, their retention in cells, and all the biological effects leading to tumor cell death.

The present work was a preliminary study to characterize new core-shell nanoparticles and evaluate their biological impact on tumor cells. To complete this work, it would be important to evaluate the effects of these nanoparticles on an animal model to characterize their stability, *in vivo* toxicity, and interactions with tissues, cells, and cellular components. Moreover, determining the optimal route/method of administration to target tumors efficiently is another challenge in nanomedicine.

As previously exposed, literature data reported promising results about the physicochemical properties of nanoparticles as potential theragnostic agents in the fight against cancer. However, there is still a research gap between generated *in vitro* and *in vivo* results and commercial requirements. It appears crucial to improve synthesis processes to fit with large-scale production while considering environmental issues. The market size of cancer therapies continues to increase, and the large-scale production of nanoparticles is still very expensive. On the other hand, researchers must strengthen the understanding of nanoparticle mechanisms through *in vitro* and pre-clinical studies to correlate these data, completely highlight nanoparticle interest, and justify related costs.

## Ethics statement

The human NF-κB-SEAP & IRF-Luc Reporter lung carcinoma cells (A549-Dual™ cells) were purchased from InvivoGen (a549d-nfis, Toulouse, France).

Review and approval by an ethics committee was not needed for this study because the present study only used a cellular model.

## Funding

This research received no specific grant from funding agencies in the public, commercial, or not-for-profit sectors.

## Data availability statement

All the data and materials are included in the present manuscript.

## CRediT authorship contribution statement

**Youssef Slama:** Writing – review & editing, Writing – original draft, Methodology, Investigation, Conceptualization. **Angelique Arcambal:** Validation, Methodology, Investigation. **Axelle Septembre-Malaterre:** Validation, Methodology, Investigation. **Anne-Laure Morel:** Methodology, Investigation. **Sabrina Pesnel:** Methodology. **Philippe Gasque:** Visualization, Validation, Supervision, Conceptualization.

## Declaration of competing interest

The authors declare that they have no known competing financial interests or personal relationships that could have appeared to influence the work reported in this paper.

## References

[1] H. Sung, J. Ferlay, R.L. Siegel, M. Laversanne, I. Soerjomataram, A. Jemal, F. Bray, Global cancer statistics 2020: GLOBOCAN estimates of incidence and mortality worldwide for 36 cancers in 185 countries, CA. Cancer J. Clin. 71 (2021) 209–249, https://doi.org/10.3322/caac.21660.

[2] IQVIA Institute, Global Oncology Trends 2023: Outlook to 2027, IQVIA Institute for Human Data Science, 2023.

[3] A. Spoială, C.-I. Ilie, L. Motelica, D. Ficai, A. Semenescu, O.-C. Oprea, A. Ficai, Smart magnetic drug delivery systems for the treatment of cancer, Nanomaterials 13 (2023) 876, https://doi.org/10.3390/nano13050876.

[4] Z. Zou, H. Chang, H. Li, S. Wang, Induction of reactive oxygen species: an emerging approach for cancer therapy, Apoptosis 22 (2017) 1321–1335, https://doi.org/10.1007/s10495-017-1424-9.

[5] A. Tulard, Persistent oxidative stress after ionizing radiation is involved in inherited radiosensitivity, Free Radic. Biol. Med. 35 (2003) 68–77, https://doi.org/10.1016/S0891-5849(03)00243-0.

[6] J.K. Leach, G.V. Tuyle, P.-S. Lin, R. Schmidt-Ullrich, R.B. Mikkelsen, Ionizing radiation-induced, mitochondria-dependent generation of reactive oxygen/nitrogen, Cancer Res. 61 (2001) 3894–3901.

[7] M. Yoshizumi, T. Nakamura, M. Kato, T. Ishioka, K. Kozawa, K. Wakamatsu, H. Kimura, Release of cytokines/chemokines and cell death in UVB-irradiated human keratinocytes, HaCaT, Cell Biol. Int. 32 (2008) 1405–1411, https://doi.org/10.1016/j.cellbi.2008.08.011.

[8] A. Brandmaier, S.C. Formenti, The impact of radiation therapy on innate and adaptive tumor immunity, Semin. Radiat. Oncol. 30 (2020) 139–144, https://doi.org/10.1016/j.semradonc.2019.12.005.

[9] G. Huang, H. Chen, Y. Dong, X. Luo, H. Yu, Z. Moore, E.A. Bey, D.A. Boothman, J. Gao, Superparamagnetic iron oxide nanoparticles: amplifying ROS stress to improve anticancer drug efficacy, Theranostics 3 (2013) 116–126, https://doi.org/10.7150/thno.5411.

[10] D. De Ruysscher, G. Niedermann, N.G. Burnet, S. Siva, A.W.M. Lee, F. Hegi-Johnson, Radiotherapy toxicity, Nat. Rev. Dis. Primer 5 (2019) 13, https://doi.org/10.1038/s41572-019-0064-5.

[11] C. Mirjolet, I. Diallo, A. Bertaut, C. Veres, P. Sargos, S. Helfre, M.-P. Sunyach, G. Truc, C. Le Pechoux, A. Paumier, A. Ducassou, M. Jolnerovski, J. Thariat, M. Lapeyre, A. Cordoba, M.-A. Mahé, P. Maingon, Treatment related factors associated with the risk of breast radio-induced-sarcoma, Radiother. Oncol. 171 (2022) 14–21, https://doi.org/10.1016/j.radonc.2022.04.004.

[12] É. Cohen-Jonathan-Moyal, V. Vendrely, L. Motte, J. Balosso, J. Thariat, Radioresistant tumours: from identification to targeting, Cancer Radiother. 24 (2020) 699–705, https://doi.org/10.1016/j.canrad.2020.05.005.

[13] D.R. Owen, P.S. Boonstra, B.L. Viglianti, J.M. Balter, M.J. Schipper, W.C. Jackson, I. El Naqa, S. Jolly, R.K. Ten Haken, F.-M.S. Kong, M.M. Matuszak, Modeling patient-specific dose-function response for enhanced characterization of personalized functional damage, Int. J. Radiat. Oncol. 102 (2018) 1265–1275, https://doi.org/10.1016/j.ijrobp.2018.05.049.

[14] T. Zhuang, N.M. Woody, H. Liu, S. Cherian, C.A. Reddy, P. Qi, A. Magnelli, T. Djemil, K.L. Stephans, P. Xia, G.M. Videtic, Dosimetric differences between local failure and local controlled non-small cell lung cancer patients treated with stereotactic body radiotherapy: a matched-pair study, J. Med. Imaging Radiat. Oncol. 62 (2018) 420–424, https://doi.org/10.1111/1754-9485.12706.

[15] V.W.C. Wu, K. Tam, S. Tong, Evaluation of the influence of tumor location and size on the difference of dose calculation between Ray Tracing algorithm and Fast Monte Carlo algorithm in stereotactic body radiotherapy of non-small cell lung cancer using CyberKnife, J. Appl. Clin. Med. Phys. 14 (2013) 68–78, https://doi.org/10.1120/jacmp.v14i5.4280.

[16] J. Ramroth, D.J. Cutter, S.C. Darby, G.S. Higgins, P. McGale, M. Partridge, C.W. Taylor, Dose and fractionation in radiation therapy of curative intent for non-small cell lung cancer: meta-analysis of randomized trials, Int. J. Radiat. Oncol. 96 (2016) 736–747, https://doi.org/10.1016/j.ijrobp.2016.07.022.

[17] A. Bezjak, R. Paulus, L.E. Gaspar, R.D. Timmerman, W.L. Straube, W.F. Ryan, Y.I. Garces, A.T. Pu, A.K. Singh, G.M. Videtic, R.C. McGarry, P. Iyengar, J. R. Pantarotto, J.J. Urbanic, A.Y. Sun, M.E. Daly, I.S. Grills, P. Sperduto, D.P. Normolle, J.D. Bradley, H. Choy, Safety and efficacy of a five-fraction stereotactic body radiotherapy schedule for centrally located non–small-cell lung cancer: NRG Oncology/RTOG 0813 trial, J. Clin. Oncol. 37 (2019) 1316–1325, https://doi.org/10.1200/JCO.18.00622.

[18] S. Jain, J.A. Coulter, A.R. Hounsell, K.T. Butterworth, S.J. McMahon, W.B. Hyland, M.F. Muir, G.R. Dickson, K.M. Prise, F.J. Currell, J.M. O'Sullivan, D.G. Hirst, Cell-specific radiosensitization by gold nanoparticles at megavoltage radiation energies, Int. J. Radiat. Oncol. 79 (2011) 531–539, https://doi.org/10.1016/j.ijrobp.2010.08.044.

[19] T. Tanaka, S. Shiramoto, M. Miyashita, Y. Fujishima, Y. Kaneo, Tumor targeting based on the effect of enhanced permeability and retention (EPR) and the mechanism of receptor-mediated endocytosis (RME), Int. J. Pharm. 277 (2004) 39–61, https://doi.org/10.1016/j.ijpharm.2003.09.050.

[20] J. Zhao, P. Liu, J. Ma, D. Li, H. Yang, W. Chen, Y. Jiang, Enhancement of radiosensitization by silver nanoparticles functionalized with polyethylene glycol and aptamer As1411 for glioma irradiation therapy, Int. J. Nanomedicine 14 (2019) 9483–9496, https://doi.org/10.2147/IJN.S224160.

[21] M. Könczöl, A. Weiss, E. Stangenberg, R. Gminski, M. Garcia-Käufer, R. Gieré, I. Merfort, V. Mersch-Sundermann, Cell-cycle changes and oxidative stress response to magnetite in A549 human lung cells, Chem. Res. Toxicol. 26 (2013) 693–702, https://doi.org/10.1021/tx300503q.

[22] H. Moustaoui, D. Movia, N. Dupont, N. Bouchemal, S. Casale, N. Djaker, P. Savarin, A. Prina-Mello, M.L. de la Chapelle, J. Spadavecchia, Tunable design of gold (III)–Doxorubicin complex–PEGylated nanocarrier. The golden doxorubicin for oncological applications, ACS Appl. Mater. Interfaces 8 (2016) 19946–19957, https://doi.org/10.1021/acsami.6b07250.

[23] A. Bindoli, M.P. Rigobello, G. Scutari, C. Gabbiani, A. Casini, L. Messori, Thioredoxin reductase: a target for gold compounds acting as potential anticancer drugs, Coord. Chem. Rev. 253 (2009) 1692–1707, https://doi.org/10.1016/j.ccr.2009.02.026.

[24] M. Watanabe, M. Yoneda, A. Morohashi, Y. Hori, D. Okamoto, A. Sato, D. Kurioka, T. Nittami, Y. Hirokawa, T. Shiraishi, K. Kawai, H. Kasai, Y. Totsuka, Effects of Fe3O4 magnetic nanoparticles on A549 cells, Int. J. Mol. Sci. 14 (2013) 15546–15560, https://doi.org/10.3390/ijms140815546.

[25] A. Espinosa, R. Di Corato, J. Kolosnjaj-Tabi, P. Flaud, T. Pellegrino, C. Wilhelm, Duality of iron oxide nanoparticles in cancer therapy: amplification of heating efficiency by magnetic hyperthermia and photothermal bimodal treatment, ACS Nano 10 (2016) 2436–2446, https://doi.org/10.1021/acsnano.5b07249.

[26] S. Gurunathan, J. Han, J.H. Park, J.-H. Kim, A green chemistry approach for synthesizing biocompatible gold nanoparticles, Nanoscale Res. Lett. 9 (2014) 248, https://doi.org/10.1186/1556-276X-9-248.

[27] A. Radomska, J. Leszczyszyn, M.W. Radomski, The nanopharmacology and nanotoxicology of nanomaterials: new opportunities and challenges, Adv. Clin. Exp. Med. Off. Organ Wroclaw Med. Univ. 25 (2016) 151–162, https://doi.org/10.17219/acem/60879.

[28] J. Estelrich, M.J. Sánchez-Martín, M.A. Busquets, Nanoparticles in magnetic resonance imaging: from simple to dual contrast agents, Int. J. Nanomedicine 10 (2015) 1727–1741, https://doi.org/10.2147/IJN.S76501.

[29] R. Ouvinha de Oliveira, L.C. de Santa Maria, G. Barratt, Nanomedicine and its applications to the treatment of prostate cancer, Ann. Pharm. Fr. 72 (2014) 303–316, https://doi.org/10.1016/j.pharma.2014.04.006.

[30] null Neetika, M. Sharma, P. Thakur, P. Gaur, G.M. Rani, S. Rustagi, R.K. Talreja, V. Chaudhary, Cancer treatment and toxicity outlook of nanoparticles, Environ. Res. 237 (2023) 116870, https://doi.org/10.1016/j.envres.2023.116870.

[31] A.-L. Morel, S.I. Nikitenko, K. Gionnet, A. Wattiaux, J. Lai-Kee-Him, C. Labrugere, B. Chevalier, G. Deleris, C. Petibois, A. Brisson, M. Simonoff, Sonochemical approach to the synthesis of Fe $_3$ O $_4$ @SiO $_2$ Core−Shell nanoparticles with tunable properties, ACS Nano 2 (2008) 847–856, https://doi.org/10.1021/nn800091q.

[32] S. Khoei, S.R. Mahdavi, H. Fakhimikabir, A. Shakeri-Zadeh, A. Hashemian, The role of iron oxide nanoparticles in the radiosensitization of human prostate carcinoma cell line DU145 at megavoltage radiation energies, Int. J. Radiat. Biol. 90 (2014) 351–356, https://doi.org/10.3109/09553002.2014.888104.

[33] F. Tabatabaie, R. Franich, B. Feltis, M. Geso, Oxidative damage to mitochondria enhanced by ionising radiation and gold nanoparticles in cancer cells, Int. J. Mol. Sci. 23 (2022) 6887, https://doi.org/10.3390/ijms23136887.

[34] A. Arcambal, J. Taïlé, P. Rondeau, W. Viranaïcken, O. Meilhac, M.-P. Gonthier, Hyperglycemia modulates redox, inflammatory and vasoactive markers through specific signaling pathways in cerebral endothelial cells: insights on insulin protective action, Free Radic. Biol. Med. 130 (2019) 59–70, https://doi.org/10.1016/j.freeradbiomed.2018.10.430.

[35] L.J. Kuo, L.-X. Yang, Gamma-H2AX - a novel biomarker for DNA double-strand breaks, Vivo Athens Greece 22 (2008) 305–309.

[36] V. Chaudhary, null Sonu, R. Chowdhury, P. Thukral, D. Pathania, S. Saklani, null Lucky, S. Rustagi, A. Gautam, Y.K. Mishra, P. Singh, A. Kaushik, Biogenic green metal nano systems as efficient anti-cancer agents, Environ. Res. 229 (2023) 115933, https://doi.org/10.1016/j.envres.2023.115933.

[37] S. Gavas, S. Quazi, T.M. Karpiński, Nanoparticles for cancer therapy: current progress and challenges, Nanoscale Res. Lett. 16 (2021) 173, https://doi.org/10.1186/s11671-021-03628-6.

[38] X. Shan, X. Gong, J. Li, J. Wen, Y. Li, Z. Zhang, Current approaches of nanomedicines in the market and various stage of clinical translation, Acta Pharm. Sin. B 12 (2022) 3028–3048, https://doi.org/10.1016/j.apsb.2022.02.025.

[39] V. Chaudhary, A. Kaushik, H. Furukawa, A. Khosla, Review—towards 5th generation AI and IoT driven sustainable intelligent sensors based on 2D MXenes and borophene, ECS Sens. Plus 1 (2022) 013601, https://doi.org/10.1149/2754-2726/ac5ac6.

[40] Polaris Market Research, Global Metal Nanoparticles Market Size, Share Analysis Report, 2022-2030, Polaris (n.d.). https://www.polarismarketresearch.com/industry-analysis/metal-nanoparticles-market (accessed March 20, 2024).

[41] G. Schmid, The relevance of shape and size of Au55 clusters, Chem. Soc. Rev. 37 (2008) 1909–1930, https://doi.org/10.1039/b713631p.

[42] Y. Wang, X. Liu, S. Ma, X. He, C. Guo, Z. Liang, Y. Hu, Y. Wei, X. Lian, D. Huang, Progress in cancer therapy with functionalized Fe3O4 nanomaterials, Front. Mater. Sci. 17 (2023) 230658, https://doi.org/10.1007/s11706-023-0658-4.

[43] Y.R. Mukhortova, A.S. Pryadko, R.V. Chernozem, I.O. Pariy, E.A. Akoulina, I.V. Demianova, I.I. Zharkova, Y.F. Ivanov, D.V. Wagner, A.P. Bonartsev, R. A. Surmenev, M.A. Surmeneva, Fabrication and characterization of a magnetic biocomposite of magnetite nanoparticles and reduced graphene oxide for biomedical applications, Nano-Struct, Nano-Objects 29 (2022) 100843, https://doi.org/10.1016/j.nanoso.2022.100843.

[44] K.I. Dhanalekshmi, K. Sangeetha, P. Magesan, J. Johnson, X. Zhang, K. Jayamoorthy, Photodynamic cancer therapy: role of Ag- and Au-based hybrid nano-photosensitizers, J. Biomol. Struct. Dyn. 40 (2022) 4766–4773, https://doi.org/10.1080/07391102.2020.1858965.

[45] J.T. Jenkins, D.L. Halaney, K.V. Sokolov, L.L. Ma, H.J. Shipley, S. Mahajan, C.L. Louden, R. Asmis, T.E. Milner, K.P. Johnston, M.D. Feldman, Excretion and toxicity of gold–iron nanoparticles, Nanomedicine Nanotechnol. Biol. Med. 9 (2013) 356–365, https://doi.org/10.1016/j.nano.2012.08.007.

[46] S. Rajkumar, M. Prabaharan, Chapter 29 - theranostic application of Fe3O4–Au hybrid nanoparticles, in: S. Mohapatra, T.A. Nguyen, P. Nguyen-Tri (Eds.), Noble Met.-Met. Oxide Hybrid Nanoparticles, Woodhead Publishing, 2019, pp. 607–623, https://doi.org/10.1016/B978-0-12-814134-2.00029-2.

[47] M.A.M. Tarkistani, V. Komalla, V. Kayser, Recent advances in the use of iron–gold hybrid nanoparticles for biomedical applications, Nanomaterials 11 (2021) 1227, https://doi.org/10.3390/nano11051227.
[48] R. Hu, M. Zheng, J. Wu, C. Li, D. Shen, D. Yang, L. Li, M. Ge, Z. Chang, W. Dong, Core-shell magnetic gold nanoparticles for magnetic field-enhanced radiophotothermal therapy in cervical cancer, Nanomaterials 7 (2017) 111, https://doi.org/10.3390/nano7050111.
[49] B. Babaye Abdollahi, M. Ghorbani, H. Hamishehkar, R. Malekzadeh, A. Farajollahi, Synthesis and characterization of actively HER-2 Targeted Fe3O4@Au nanoparticles for molecular radiosensitization of breast cancer, BioImpacts BI 13 (2023) 17–29, https://doi.org/10.34172/bi.2022.23682.
[50] H.K. Patra, S. Banerjee, U. Chaudhuri, P. Lahiri, A.Kr Dasgupta, Cell selective response to gold nanoparticles, Nanomedicine Nanotechnol. Biol. Med. 3 (2007) 111–119, https://doi.org/10.1016/j.nano.2007.03.005.
[51] S. Alarifi, D. Ali, S. Alkahtani, M.S. Alhader, Iron oxide nanoparticles induce oxidative stress, DNA damage, and caspase activation in the human breast cancer cell line, Biol. Trace Elem. Res. 159 (2014) 416–424, https://doi.org/10.1007/s12011-014-9972-0.
[52] T. Sun, Y. Yan, Y. Zhao, F. Guo, C. Jiang, Copper oxide nanoparticles induce autophagic cell death in A549 cells, PLoS One 7 (2012) e43442, https://doi.org/10.1371/journal.pone.0043442.
[53] K.T. Butterworth, S.J. McMahon, L.E. Taggart, K.M. Prise, Radiosensitization by gold nanoparticles: effective at megavoltage energies and potential role of oxidative stress, Transl, Cancer Res. 2 (2013) 11.
[54] P. Liu, Z. Huang, Z. Chen, R. Xu, H. Wu, F. Zang, C. Wang, N. Gu, Silver nanoparticles: a novel radiation sensitizer for glioma? Nanoscale 5 (2013) 11829–11836, https://doi.org/10.1039/C3NR01351K.
[55] R. Mohammadinejad, M.A. Moosavi, S. Tavakol, D.Ö. Vardar, A. Hosseini, M. Rahmati, L. Dini, S. Hussain, A. Mandegary, D.J. Klionsky, Necrotic, apoptotic and autophagic cell fates triggered by nanoparticles, Autophagy 15 (2019) 4–33, https://doi.org/10.1080/15548627.2018.1509171.
[56] H. Nosrati, M. Salehiabar, J. Charmi, K. Yaray, M. Ghaffarlou, E. Balcioglu, Y.N. Ertas, Enhanced in vivo radiotherapy of breast cancer using gadolinium oxide and gold hybrid nanoparticles, ACS Appl. Bio Mater. 6 (2023) 784–792, https://doi.org/10.1021/acsabm.2c00965.
[57] L.O. Abdelhakm, E.I. Kandil, S.Z. Mansour, S.M. El-Sonbaty, Chrysin encapsulated copper nanoparticles with low dose of gamma radiation elicit tumor cell death through p38 MAPK/NF-κB pathways, Biol. Trace Elem. Res. (2023), https://doi.org/10.1007/s12011-023-03596-1.
[58] C. Gräfe, A. Weidner, M.v.d. Lühe, C. Bergemann, F.H. Schacher, J.H. Clement, S. Dutz, Intentional formation of a protein corona on nanoparticles: serum concentration affects protein corona mass, surface charge, and nanoparticle–cell interaction, Int. J. Biochem. Cell Biol. 75 (2016) 196–202, https://doi.org/10.1016/j.biocel.2015.11.005.
[59] M. Hullo, R. Grall, Y. Perrot, C. Mathé, V. Ménard, X. Yang, S. Lacombe, E. Porcel, C. Villagrasa, S. Chevillard, E. Bourneuf, Radiation enhancer effect of platinum nanoparticles in breast cancer cell lines: in vitro and in silico analyses, Int. J. Mol. Sci. 22 (2021) 4436, https://doi.org/10.3390/ijms22094436.
[60] D. Howard, S. Sebastian, Q.V.-C. Le, B. Thierry, I. Kempson, Chemical mechanisms of nanoparticle radiosensitization and radioprotection: a review of structure-function relationships influencing reactive oxygen species, Int. J. Mol. Sci. 21 (2020) 579, https://doi.org/10.3390/ijms21020579.
[61] T. Yamamori, H. Yasui, M. Yamazumi, Y. Wada, Y. Nakamura, H. Nakamura, O. Inanami, Ionizing radiation induces mitochondrial reactive oxygen species production accompanied by upregulation of mitochondrial electron transport chain function and mitochondrial content under control of the cell cycle checkpoint, Free Radic. Biol. Med. 53 (2012) 260–270, https://doi.org/10.1016/j.freeradbiomed.2012.04.033.
[62] P. Ma, H. Xiao, C. Yu, J. Liu, Z. Cheng, H. Song, X. Zhang, C. Li, J. Wang, Z. Gu, J. Lin, Enhanced cisplatin chemotherapy by iron oxide nanocarrier-mediated generation of highly toxic reactive oxygen species, Nano Lett. 17 (2017) 928–937, https://doi.org/10.1021/acs.nanolett.6b04269.
[63] P. Retif, S. Pinel, M. Toussaint, C. Frochot, R. Chouikrat, T. Bastogne, M. Barberi-Heyob, Nanoparticles for radiation therapy enhancement: the key parameters, Theranostics 5 (2015) 1030–1044, https://doi.org/10.7150/thno.11642.
[64] K. Haume, S. Rosa, S. Grellet, M.A. Śmiałek, K.T. Butterworth, A.V. Solov'yov, K.M. Prise, J. Golding, N.J. Mason, Gold nanoparticles for cancer radiotherapy: a review, Cancer Nanotechnol 7 (2016) 8, https://doi.org/10.1186/s12645-016-0021-x.
[65] N.M. Dimitriou, G. Tsekenis, E.C. Balanikas, A. Pavlopoulou, M. Mitsiogianni, T. Mantso, G. Pashos, A.G. Boudouvis, I.N. Lykakis, G. Tsigaridas, M. I. Panayiotidis, V. Yannopapas, A.G. Georgakilas, Gold nanoparticles, radiations and the immune system: current insights into the physical mechanisms and the biological interactions of this new alliance towards cancer therapy, Pharmacol. Ther. 178 (2017) 1–17, https://doi.org/10.1016/j.pharmthera.2017.03.006.
[66] K.M. Arnold, L.M. Opdenaker, N.J. Flynn, D.K. Appeah, J. Sims-Mourtada, Radiation induces an inflammatory response that results in STAT3-dependent changes in cellular plasticity and radioresistance of breast cancer stem-like cells, Int. J. Radiat. Biol. 96 (2020) 434–447, https://doi.org/10.1080/09553002.2020.1705423.
[67] A. Alkhatib, Y. Watanabe, J.H. Broadhurst, The local enhancement of radiation dose from photons of MeV energies obtained by introducing materials of high atomic number into the treatment region: dose enhancement by high-Z material for photon radiotherapy, Med. Phys. 36 (2009) 3543–3548, https://doi.org/10.1118/1.3168556.
[68] B.L. Jones, S. Krishnan, S.H. Cho, Estimation of microscopic dose enhancement factor around gold nanoparticles by Monte Carlo calculations: microscopic dose enhancement factor around gold nanoparticles, Med. Phys. 37 (2010) 3809–3816, https://doi.org/10.1118/1.3455703.